Small-Particle Size Determination by Optical Array Probe Oversampling

A. R. D. SMEDLEY, C. P. R. SAUNDERS, AND A. R. WEBB

University of Manchester Institute of Science and Technology, Manchester, United Kingdom

(Manuscript received 31 July 2002, in final form ?? ?? 2003)

ABSTRACT

Oversampling of optical array probes (OAPs) is described as a novel technique to increase the quality of small-particle data available in cloud microphysics. The slice rate of a 10-μm-resolution grayscale OAP is increased by a factor f with respect to that which would produce images with an aspect ratio of 1:1 for the given air velocity and probe resolution. The Fresnel diffraction pattern is simulated and the probe response calculated for normal ($f = 1$) and oversampled ($f = 10$) cases. The increased number of pixels imaged by the OAP permits the fraction of 25%–50% shadowed pixels to be used to obtain a much improved estimate of the actual droplet diameter for droplets between 7 and 50 μm in diameter. The process of oversampling is also found to significantly increase the sample area for the smallest particles. Example laboratory particle size distributions are provided. The oversampling factor for an individual probe is limited by the maximum sampling frequency, the airspeed, and the probe resolution.

1. Introduction

Optical array probes (OAPs) have become an important tool in obtaining detailed measurements of cloud particles since their inception over three decades ago (Knollenberg 1970) and remain so despite more recent developments (Lawson and Cormack 1995; Lawson et al. 1998). During this period a number of different models of OAPs have been developed, all relying on the same principle: as a particle traverses an elliptical beam of radiation its shadow falls upon a linear array of photodiodes. In grayscale probes the amplified photodiode signals, normalized by their background intensities, are encoded as levels of intensity to form a single image slice. Probes are habitually set up to record image slices at a rate proportional to the movement of air through the sample area to ensure that the complete recorded image preserves the cross-sectional shape of the particle in question. Raw images are then analyzed to obtain typical microphysical properties. The first stage of analysis rejects invalid images according to several criteria, including the depth of field. The remaining particle images are sized and normalized by the sample area to form the size distribution.

The relative simplicity of this process, together with the rapid production of particle size spectra, is convenient and offers obvious advantages over earlier methods of measuring cloud microphysical properties. However, this obscures two main limitations of probes, namely, the accuracy of both sizing particles and estimating sample areas.

A number of authors have investigated particle sizing by probes. Hovenac and Hirleman (1991) showed that the measured particle size varied with distance from the focal plane during laboratory calibrations with a rotating reticule. The measured size was found to be a nonmonotonic function of distance from the focal plane and dependent on the actual size of the particle being observed. Korolev et al. (1991) provided a theoretical explanation of these findings and demonstrated that shadow images of spherical droplets could be modeled by Fresnel diffraction by an opaque disc. Korolev et al. (1998) continued this work and showed that a 25-μm probe can both over- and undersize droplets smaller than 100-μm diameter and oversize those above this threshold. Reuter and Bakan (1998) carried out test measurements with a spinning glass disc with sample spots. A method was proposed to improve the estimation of the nominal particle size by comparing the number of pixels shadowed at the lowest threshold to the total number shadowed, which provided an estimation of the droplet's distance from the object plane. This allowed a 10-μm grayscale probe to estimate the sizes of 50–500-μm droplets with an rms uncertainty of less than 6%. The studies by Korolev et al. (1998) and Reuter and Bakan (1998) will be referenced a number of times and thus will be referred to as KEA and RB, respectively.

Knollenberg (1970) first gave the effective depth of field (DOF) for the shadow image of a spherical particle. However, Heymsfield and Baumgardner (1985) reported

Corresponding author address: Andrew R. D. Smedley, Atmospheric Physics Research Group, Department of Physics, UMIST, P.O. Box 88, Sackville St., Manchester, M60 1QD, United Kingdom.
E-mail: andrew.smedley@umist.ac.uk

that the DOF found in tests can commonly be 2 or 3 times the theoretical value, with this issue being the primary uncertainty in determining sample area for particles less than 240 μm in diameter. Korolev et al. (1991) showed that the sample area has a sawtooth structure due to the oscillations in the particle diameter as estimated from 50% shadow pixels, although these investigations were carried out only for larger particles. KEA showed that the counting losses due to the discrete nature of the particle image recording increase with decreasing size and reach 70% for 25-μm droplets, with the counting efficiency exhibiting a complicated structure for particles less than 100 μm. However, Brown and Francis (1995), in a comparison between a new fast response water vapor sensor and a 2D probe, noted no tendency for the ice water content ratio between the two instruments to decrease for droplets below 50 μm. Such a tendency would be expected if the 2D probe was systematically undercounting the concentration of crystals smaller than 150 μm.

The estimation of both these variables becomes less accurate at small particle sizes, as first noted by Curry and Schemenaur (1979) and reflected by researchers' attitudes toward 2DC probe data below 100 μm (Heymsfield and Baumgardner 1985).

Two further aspects of probe data analysis should be noted at this point, although they are not incorporated into this work. First, the photodetectors have a nonzero response time that Gayet et al. (1993) found to be 0.3 μs for 2DC probes compared to 1.0 μs for the newer 2D2C model. This requires the length of particles to be increased by 1.0–1.5 times the array resolution (Heymsfield and Baumgardner 1985), a value that depends on the air velocity at the probe tips. The nonzero response time also significantly reduces the small-particle depth of field at high airspeeds with the value for individual photodiodes ranging from 0.44 to 0.90 μs (Strapp et al. 2001). Second, as reported by these authors, the shadow threshold intensity can vary significantly, whereas it is usually presumed to be 50% for particle sizing purposes. Most recently Jensen and Granek (2002) convolved a modeled optical field with the electronic response function to simulate the electrical signal as a droplet passes the probe. Although that study relates to a 260X probe and concerns much larger droplets than those considered here, the bias toward increased depths of field for larger particles and reduced depths of field for high airspeeds is of note. A full treatment should include the effect of the electronic response time, although here it has been omitted for the sake of clarity and the greater applicability of oversampling to lower airspeeds.

It is apparent that small particles are notoriously difficult to size, and the complete particle size distribution is sometimes misrepresentative of the true cloud properties. The aim of this paper is to demonstrate the usefulness of oversampling cloud droplets to increase the accuracy of grayscale probe measurements at small droplet diameters. The method of KEA is followed to simulate the shadowgraphs formed by droplets. These are then sampled as would be done by an idealized 10-μm-resolution grayscale probe (ignoring response time and imperfect threshold effects) both for a pixel aspect ratio of 1.0, which is typical, and by increasing the slice rate frequency so that the pixel aspect ratio is increased by a factor of 10. This factor is that used in the probe's laboratory setting and provides a useful compromise between excessively long images and improved sizing capabilities. The effect of random droplet positioning with respect to the array is included. Thus probe images are simulated for both cases with known droplet diameters and positions. These images are then sized by two alternative methods to give mean estimates of the particle size as a function of particle size and distance from the focal plane. Reuter and Bakan's method is applied to oversampled droplet images to obtain corrected diameters, and the calculated depth of field is shown. Results from a real probe using the oversampled method are presented and discussed.

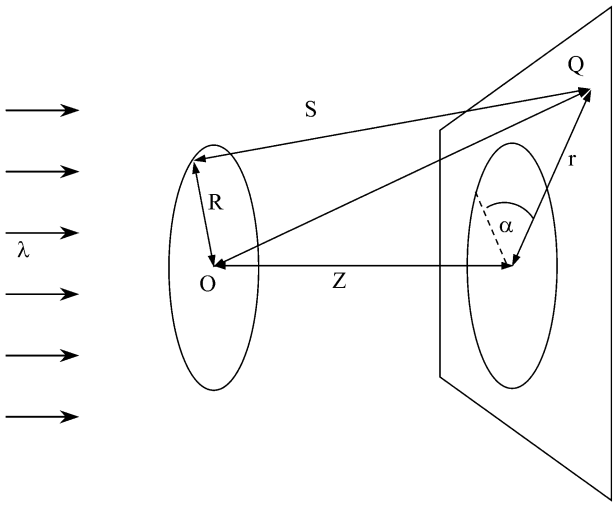

FIG. 1. Fresnel diffraction by an opaque disc showing definitions of variables.

2. Formation of diffraction images by droplets

The image produced due to the interaction of a water droplet with a laser beam of wavelength 632.8 nm can be modeled well by Fresnel diffraction by an opaque disc (Korolev et al. 1991). This approximation assumes that the refracted component of the light can be ignored because the droplets act as short focus lenses. Additionally, it is assumed that the diffraction by an opaque sphere is approximated by that from its geometric shadow. The details are reproduced here for completeness.

The intensity of light at a point Q (Fig. 1) is considered to be the sum of a boundary wave and an incident wave and is given as

$$I(\xi) = |U_g(\xi) + U_d(\xi)|^2, \quad (1)$$

where

$$U_g(\xi) = \begin{cases} \exp(ikZ) & \text{if Q lies in the direct beam,} \\ 0 & \text{if Q lies in the geometric shadow,} \end{cases} \quad (2)$$

$$U_d(\xi) = -\frac{1}{4\pi}\int_0^{2\pi} \frac{\exp(ikS)(R^2 - Rr\cos\alpha)}{Z(S - Z)}\, d\alpha, \quad (3)$$

and where $\xi = r/R$, R is the droplet radius, r is the distance from the center of the image to point Q, $k = 2\pi/\lambda$ where λ is the wavelength, Z is distance between the center of the droplet and the focal plane, and S can be found from trigonometry to be $(Z^2 + R^2 + r^2 - 2Rr\cos\alpha)^{1/2}$. The diffraction image formed can be presented as a function of a single dimensionless variable $Z_d = \lambda|Z|/R^2$.

This analysis has been implemented into a model written in the MATLAB analysis application (The Math Works, Inc.) with normalized intensities calculated for 400 equally spaced intervals of r for $0 \leq r < 4R$. The radial symmetry of the system permits the diffraction image to be produced for all integer droplet diameters (D) between 7 and 50 μm. These were calculated for Z_d intervals of 0.1 from 0.1 to 8.2, with the focal plane diffraction image approximated by taking $Z_d = 0.02$. The upper limit in Z_d has been chosen to lay above the threshold above which the diffraction image cannot exhibit regions with intensity less than 50% (KEA). It is assumed that the optical transfer system has a negligible effect on the observed diffraction pattern, as in KEA.

At this point the different conventions in referring to the grayscale levels should be clarified. The term ''intensity level'' is defined by the ratio I/I_0, where I is the light intensity at the image point in question and I_0 is the incident light intensity. This differs form the term ''shadow level,'' which is defined as $(I - I_0)/I_0$. Later models of probes encode the data as four levels of shadow with the terms MIN, MID, and MAX equating to shadow levels of 25%–50%, 50%–75%, and greater than 75%, respectively, and intensity levels of less than 75%, less than 50%, and less than 25%, respectively. The fourth unnamed level corresponds to the background shadow intensity of less than 25%.

3. Probe sampling and quantization issues

The discrete probe image formed as a particle passes the linear photodiode array is built up in slices in a real OAP. Here though, the diffraction image has been calculated and the passage of the particle is simulated by finding the positions of photodiode centers both along the length of the array (x direction) and in the flow direction (y direction). The resolution of the probe is 10 μm, and the diodes are taken to be circular and cover an area two-thirds of that covered by square space-filling diodes, as in KEA. This corresponds to a diode with an effective radius of 4.6 μm when magnification is taken into account. Initially, a photodiode is aligned with the center of the diffraction image ($r = 0$). In the x direction neighboring array element centers are positioned every 10 μm with respect to this, and in the y direction subsequent diode centers are positioned every 10 μm in the case of normal sampling and every 1 μm for the oversampled case. The average value of all diffraction image elements that lie within 4.6 μm of each diode center are then found. It should be noted that the number of diffraction image elements within the diode field of view reduces with increasing droplet diameter. The spacing of diffraction image elements has been chosen such that at least 500 contribute to each probe image pixel value when the largest droplets are tested.

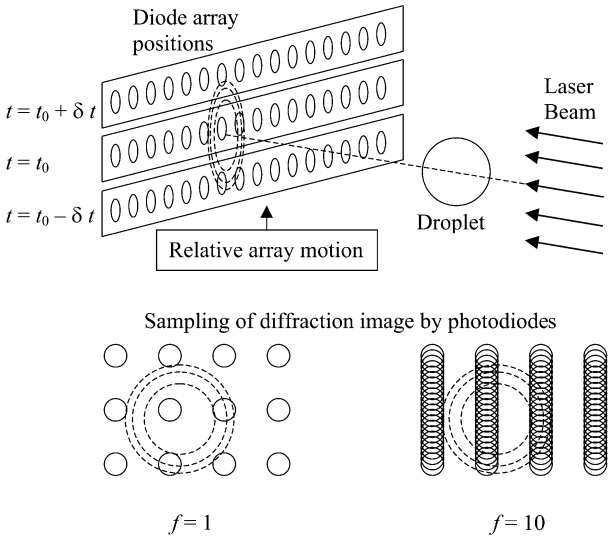

FIG. 2. Illustration of oversampling of diffraction image by photodiodes. During a time increment, δt, the photodiode array moves up relative to the diffraction pattern. In the $f = 1$ case (lower left) the diodes sample as shown; in the $f = 10$ case (lower right) the sampling is increased in the flow direction.

It is important to note that although this process forms a probe image that is extended by a factor of approximately 10 in the oversampled case, the diffraction image elements that are sampled by a single diode are the same in both instances if the diode centers coincide. The sample areas overlap in the y direction and are not compressed to ellipses (Fig. 2).

The situation described above though only provides for droplets whose centers are precisely aligned with a photodiode center. This is an important issue, as has been shown by previous authors (KEA), because a small shift in the original diffraction image with respect to the photodiode grid can cause relatively large variations in the discrete probe image. In reality, droplet centers are randomly offset from a diode center. This is simulated by repeating the sampling of the diffraction image by the probe with photodiode–droplet offsets in both the x and y directions at intervals of 0.5 μm in both directions up to half the probe resolution. The symmetry of the physical system removes the need to calculate probe

images for offsets between 5 and 10 μm. Consequently, for each D and Z_d the diffraction image is sampled 100 times, enabling a representative sample of particle diameter estimates to be obtained.

The simulation then converts each discrete probe image into one with four levels of grayscale, as would be obtained with the real probe. Although it would have been more efficient to convert the diffraction image to a two-bit image and then carry out the photodiode sampling, as done in KEA, the order used is intended to replicate that found in the OAP optical and electronic system.

4. Particle sizing

Several methods can be used to size probe images with an aspect ratio of 1:1. Those that are most applicable for small images are the diameter obtained from the maximum image width and the equivalent diameter of a circle with area equal to the total number of MID shadowed pixels (D_{edge} and D_{area} in KEA, denoted herein as d_E and d_A). Definitions of droplet diameter that involve concentric rings are not used in this study, as ring structures are not generally visible at the droplet diameters with which we are most concerned.

For oversampled probe images the above definitions are not valid and must be replaced as follows:

$$d_E = r_p\left(1 + \frac{L_{\text{sh}}}{f}\right), \tag{4}$$

$$d_A = 2r_p\left(\frac{N_{\text{sh}}}{\pi f}\right)^{1/2}, \tag{5}$$

where N_{sh} is the number of MID shadowed pixels in the probe image, L_{sh} is the length of the image along the flow direction in units of MID shadowed pixels, f is the oversampling factor, and r_p is the resolution of the probe. Additionally, the analysis of the simulated probe images records the number of probe pixels shadowed at each shadow level, enabling the proportion of MIN shadowed pixels to be found (q_{MIN}).

5. Model results and discussion

a. Particle sizing

The method of oversampling offers an immediate advantage when sizing particles in that the edge of a particle (in terms of the location of the photodiode center on the diffraction image that corresponds to the MID–MIN shadow level threshold) is defined more accurately. However, when the mean values of d_A and d_E, averaged over x and y offsets and Z_d, are calculated for $f = 1$ and 10 and plotted against the actual droplet diameter, little difference is seen between the oversampled and normal cases for $D > 12$ μm (Fig. 3). Below this threshold, both size estimates for $f = 1$ tend to the lowest available value, equivalent to a single pixel being shadowed. The oversampled cases do not suffer this restriction, and d_A is seen to provide the closest estimate of the actual droplet diameter throughout the range. There is a large spread of values that contribute to each size estimate in Fig. 3, as can be seen in Fig. 4. Here size estimates from all values of x and y offsets and Z_d are rounded to the nearest micron and plotted. The only substantial difference between histograms for each value of D is that in the $f = 1$ case the values fall into a smaller number of size intervals, but they are spread over the same range, so that, except for the smallest droplets, enough information is contained in each histogram to obtain a reasonable estimate of the diameter of the diffraction image.

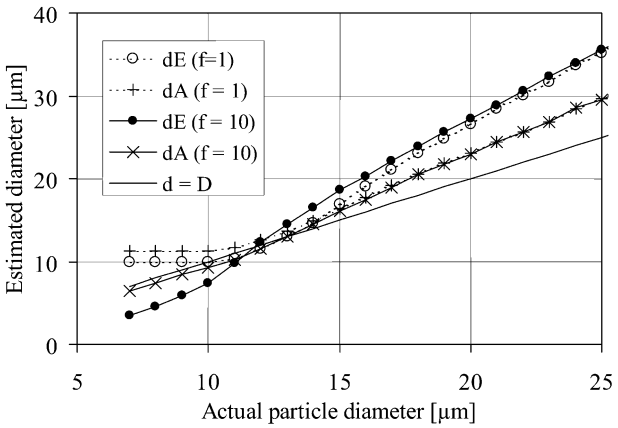

FIG. 3. Comparison of mean estimated particle sizes as a function of D. Results are only shown up to 25 μm to emphasize the region near $D = 12$ μm.

However, the diffraction image size varies considerably with distance from the focal plane and alone provides a poor estimate of the actual droplet diameter. RB attempted to solve this problem by plotting the estimated diffraction image diameter against the proportion of MIN shadowed pixels in the complete probe image (q_{MIN}). This resulted in a set of curves, one for each value of the actual droplet diameter, with each curve approximated by a linear fit. The ordinate intercept and gradient of these relations were in turn found to exhibit linear behavior with the nominal particle diameter. The result was that a single probe image could be characterized in terms of the estimated diameter and the proportion of MIN shadowed pixels, equivalent to finding Z_d and hence a much improved estimate of the actual particle diameter. The limit imposed on RB's method is the low number of pixels in the image, which for small particles has been greatly increased here by oversampling. It is clear that, unfortunately, this method cannot be applied to single-bit (mono) probe images.

The same process is carried out here. For each set of values (x, y, Z_d, D) the proportion of MIN shadowed pixels in the image is found together with the diameter as estimated from the area of all shadowed pixels (d_{25}). This last is calculated in the same way as d_A but uses

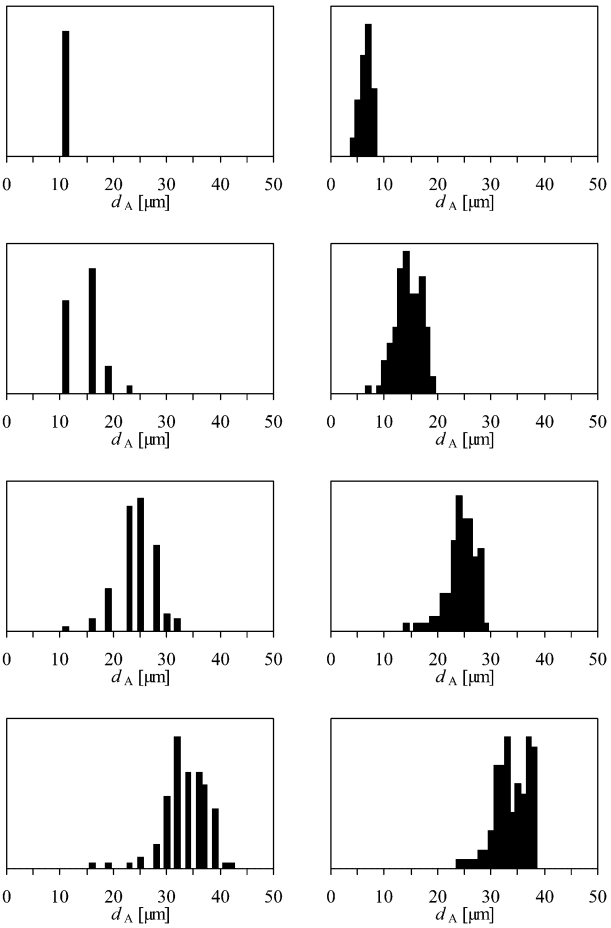

FIG. 4. Example normalized histograms illustrating the size estimates that contribute to the means plotted in Fig. 3 for oversampled and normal d_A values. Histograms are shown for $f = 1$ and 10 (left to right) and for $D = 7$, 14, 21, and 28 μm (top to bottom). The ordinates are in arbitrary units.

all MIN, MID, and MAX pixels to provide a size estimate that increases steadily with distance from the focal plane. The value of q_{MIN} also increases with Z_d, although the nature of the diffraction pattern results in a few sharp peaks. Plotting q_{MIN} against d_{25} for each value of D produces a set of curves that exhibit a large degree of structure. Figure 5 shows only a subset of these to improve clarity. A number of loops can be seen, especially for the largest values of D, resulting from the aforementioned peaks. Although aspects of this form can be seen in RB's Fig. 3, the lower number of data points in that study reduces the effect visually and improves the quality of linear fit. In this study a choice was made to continue by also using a linear fit, despite the obvious nonlinearity of the curves. The reason for this was twofold: first, although fitting, for example, a quadratic to each curve improved the situation at the first stage, the subsequent variation of each coefficient against the nominal particle diameter was also nonlinear, and the

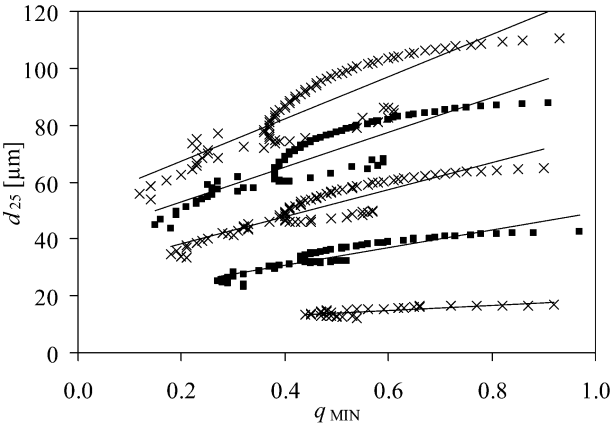

FIG. 5. Diameter estimate (d_{25}) against fraction of MIN shadowed pixels (q_{MIN}) for actual particle diameters of 10, 20, 30, 40, and 50 μm. Also shown are linear fits to each set of data for $q_{\text{MIN}} < 0.98$.

overall result showed no improvement; second, a linear fit simplified and clarified the method.

The curves are then approximated as follows:

$$d_{25} = \alpha(D)q_{\text{MIN}} + \beta(D). \tag{6}$$

The two coefficients are as plotted in Fig. 6 and as such show a nearly linear variation against the actual particle diameter and are themselves approximated by a linear fit as follows:

$$\alpha(D) = \alpha_1 D + \alpha_0 \quad \text{and} \tag{7}$$

$$\beta(D) = \beta_1 D + \beta_0. \tag{8}$$

When each fit is carried out in turn, the following values are found:

$$\alpha_1 = 1.5397, \qquad \alpha_0 = -0.3004,$$

$$\beta_1 = 1.1278, \quad \text{and} \quad \beta_0 = -4.5338.$$

As was done by RB, these equations can be re-

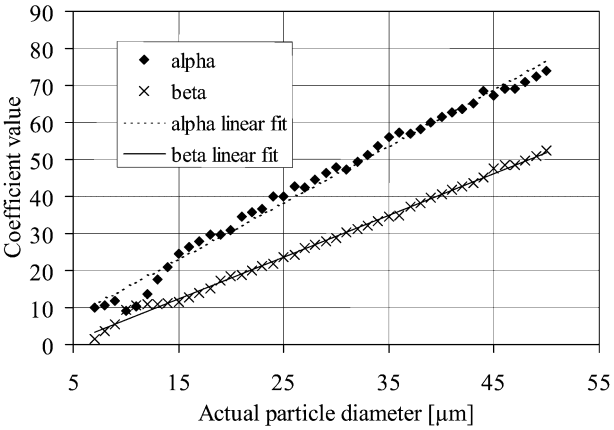

FIG. 6. Variation of coefficient values α and β against actual particle diameters for all integer values between 7 and 50 μm. Also shown are linear fits.

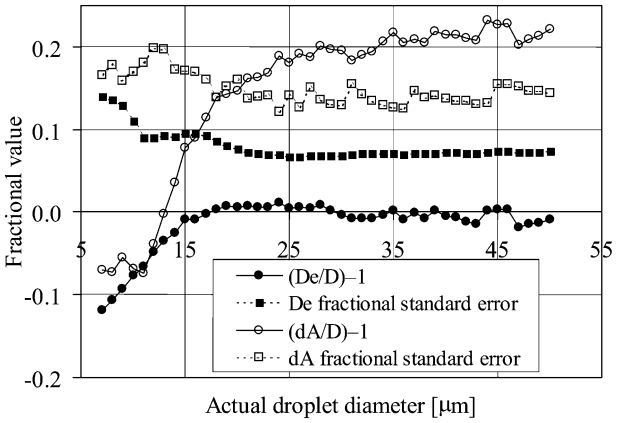

FIG. 7. Fractional standard error and fractional deviation from actual particle diameter of corrected D_e and uncorrected d_A for all integer values of D between 7 and 50 μm.

arranged to find an improved estimate of the particle diameter, D_e, in terms of q_{MIN} and d_{25}:

$$D_e = \frac{d_{25} - \alpha_0 q_{\mathrm{MIN}} - \beta_0}{\alpha_1 q_{\mathrm{MIN}} + \beta_1}. \quad (9)$$

This relation has been used to find new estimates of the droplet diameter for the full range of x and y offsets and Z_d investigated for each nominal particle diameter in turn. The fractional standard error and fractional deviation of the mean from the true value have been calculated and plotted alongside their counterparts for the uncorrected case in Fig. 7. It is clear that the corrected means adhere to the actual diameters much more closely than do the uncorrected values, with typical deviations of 2% and 20%, respectively, although for the smallest droplets the magnitudes of these become larger and smaller, respectively. The often-mentioned issue of small particles being undersized and larger ones oversized can be seen to be confirmed for uncorrected measurements. The standard errors are shown to be halved in the corrected case, with values in the region of 7% for the most part, rising to double this value for $D = 7$ μm. These improvements in sizing have particular importance for derived particle concentrations, as noted by Strapp et al. (2001); when the number count is converted to a concentration, using the sample volume, the contribution of mis-sized particles to a size interval to which the actual particle does not belong can be greatly magnified by the rapid change in sample volume between sizes.

b. Counting efficiency and depth of field

As found in previous studies, the counting efficiency exhibits a complex structure as a function of both Z_d and D when the oversampling factor is equal to 1.0 (Fig. 8a). However, when the oversampling factor is increased to 10 the complexity is reduced (Fig. 8b) and a top-hat function is found for $D > 12$ μm. This compares with

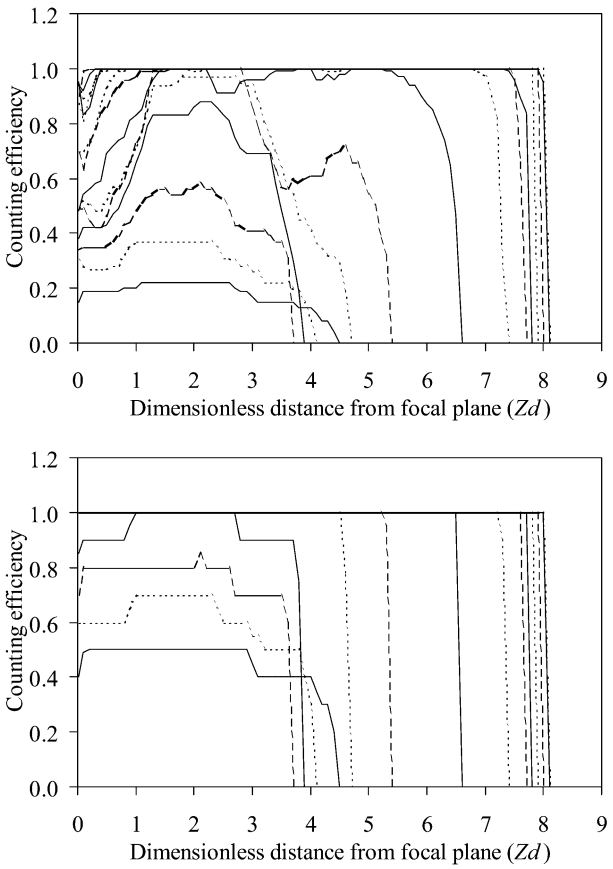

FIG. 8. Counting efficiency against droplet dimensionless distance from the focal plane for (top) $f = 1$ and (bottom) $f = 10$. Lines are shown for $D = 7$, 8, 9, 10, 11, 12, 15, 20, 25, 30, 35, 40, 45, and 50 μm with alternating line styles (solid, short dash, long dash). In the lower plot the lines for $D = 45$ and 50 μm are coincident. The lowest counting efficiencies are found for $D = 7$ μm.

a value of 35 μm in the first case. The curves in Fig. 8a are very similar to those found by KEA; most of the differences can be attributed to the probe resolution of 25 μm used in that study in comparison to 10 μm here. However, one additional feature of the graphs should be noted: there is a drop in the counting efficiency close to $Z_d = 0$ for the smallest particle sizes. As this occurs for D approximately equal to or smaller than the probe resolution, it is suggested that some degree of blurring and enlargement of the $Z_d = 0$ image is necessary (i.e., an increase in Z_d) for the OAP to register a MID shadowed pixel. Otherwise there is too great a contribution from the surrounding high-intensity area to count the particle for many of the photodiode–droplet center x and y offsets.

The early onset of a top-hat function in the oversampled case can be attributed to a full sampling of the diffraction image in the y offset direction for every probe image. Briefly, in the normal situation ($f = 1$) a small particle may or may not cause any pixels to be shadowed at the MID level as a function of the x and y

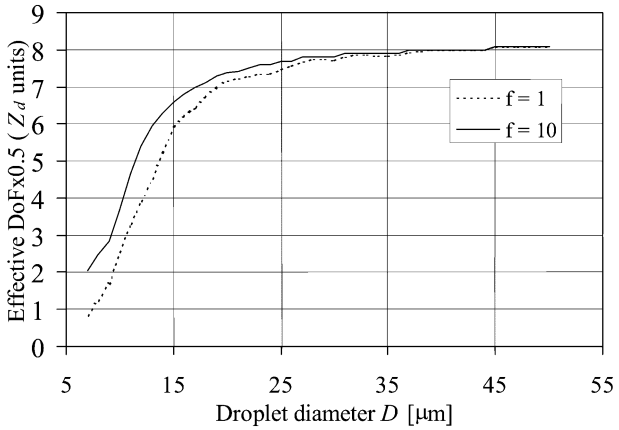

FIG. 9. Effective depth of field against true particle size found from integrating counting efficiencies for $f = 1$ and 10.

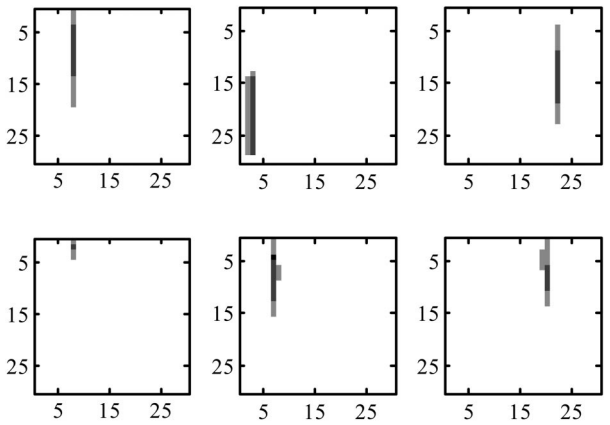

FIG. 10. Sample probe images with slice rate increased by factor of 10 for probe with 10-μm resolution.

offset values. For a single value of x a particle may or may not be counted depending on the value of y. However, for the oversampled case for a single value of x the act of oversampling causes diode centers to be positioned across the ideal diffraction image as if all values of the y offset are being sampled simultaneously. Therefore, if a particle is counted for a particular pairs of values (x_0, y_0) in the $f = 1$ case, it will be counted for all values of y with an accompanying $x = x_0$ in the $f = 10$ case. Thus, where the counting efficiency is nonzero in Fig. 8a, it is increased in Fig. 8b, and where the particle is counted at least once for each value of x in the $f = 1$ case, the counting efficiency rises to 100% in the $f = 10$ case. In our case the $f = 10$ values should be multiples of 0.1, which, for the most part, they are. There are a few points that do not follow this rule, and the reason for this is unclear. It should be noted that if values other than $f = 10$ are used, then aspects of the above argument do not hold, although there would still be an increase in the counting efficiency.

In turn the integrated depth of field (Fig. 9), together with the sample area, is increased, which causes an increase in the proportion of small particles being counted by the OAP. For the smallest particles that can be imaged by a probe the integrated depth of field is increased by a factor of 2.5, although this can be seen to drop to 1.44 for diameters of 10 μm and cause an increase of only 3% for droplets 20 μm in diameter. These improvements are relative and should be considered as only partly counteracting the effects of the increased image transfer time, which thus reduces the fraction of time in which the OAP is able to record new particles.

6. Sample measurements

For comparison, some measurements of laboratory-produced clouds are presented. The probe was positioned beneath a cloud chamber in a cold room, and air from the cloud was drawn past the probe tips before passing out of the cold room where the airspeed is measured by a digital readout vane anemometer. The measured wind speed was converted to that at the probe tips by recording the time taken to fill a known volume at the probe tips and at the anemometer, accounting for variations in the diameter of the flow tube at both points. The wind speed at the anemometer was controlled by varying the voltage supplied to the vacuum pump, and the necessary slice rate for a particle aspect ratio of 1:1 was calculated. The slice rate was then increased by a factor (f) of 10. A water cloud was produced by continuous addition of water vapor and simultaneous evacuation past the probe tips. Six 15-s samples were taken every 3 min after the first particle was imaged. For each sample a raw file was generated and the images were decoded and viewed.

In many of the experimental runs a high concentration of small particles was created, producing probe images with several groups of shadowed particles. Standard analysis methods would often reject such images, but here the groups of contiguous shadowed pixels have been identified and the presence or absence of at least one MID shadowed pixel determined. Absence of any such pixels leads to rejection of the group. The group was then tested for edge and length rejection; if any pixels in the group occurred at the limits of the array then the group was again rejected. The droplet diameters were estimated from both sizing definitions [Eqs. (4)–(5)]. Sample images of small particles that illustrate the stretching of the image in the flow direction are shown in Fig. 10. Figure 11 shows sample particle size distributions for D_e employing oversampling ($f = 10$). For comparison, the $d_A(f = 1)$ particle size distribution ordinarily obtained would consist of only three data points at sizes of 10, 20 and 30 μm, with a significant bias toward higher values.

7. Conclusions

This work demonstrates that oversampling of a 2D grayscale probe with 10-μm resolution can provide a

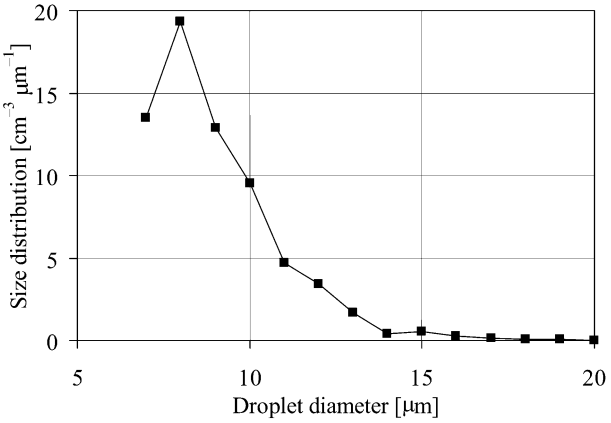

FIG. 11. Sample particle size distribution for D_e and $f = 10$.

useful means to implement the method of RB and thus obtain improved particle size distributions for droplets between 7 and 50 μm in diameter. Equivalent improvements would be found for probes with resolutions of 25 and 200 μm.

Without oversampling, the linear fit employed by RB deteriorates for the smallest droplets because of the low number of shadowed pixels. Oversampling the OAP at a factor $f = 10$ results in probe images extended in the airflow direction, increasing the number of pixels and enabling RB's method to be employed. Corrected droplet diameters result with a fractional standard error of typically 7% for droplets larger than 18 μm in diameter, rising only to 14% for the smallest observable droplets of 7-μm diameter. The mean corrected size estimates are typically within 2% of the actual particle diameter. The counting efficiency and hence the depth of field is increased for droplets with $D < 12$ μm when oversampling is used, the latter found to lie above the theoretical value suggested by Knollenberg (1970) for $D > 10$ μm, rising to an upper limit of $Z_d = 8.1$ (corresponding to the value of 8.18 noted by KEA).

It should be noted that this analysis applied to droplets only, and attempting to apply this method to ice crystals, although possibly beneficial, would introduce a large degree of extra complexity by including the effects of particle orientation, habit, and additional size parameters.

Also, it should be stressed that certain simplifications have been made in this study. The probe simulated and used had a resolution of 10 μm, and differing α and β values would be found for other probe resolutions and if different values of f were adopted. The response time of the photodiodes has been assumed to be zero, which was valid for the experimental data shown in Fig. 11 where the probe airspeed was only 0.27 m s^{-1}. Furthermore, oversampling could be severely restricted at typical aircraft speeds by the maximum probe sampling frequency. Specifically, the product of f and the airspeed must be less than the product of the maximum sampling frequency and the resolution. Subject to this restriction, the optimum choice of oversampling factor will be determined by the required particle size range and interval. For higher values of f, larger drops may not be measured, depending on the probe configuration, because of the extended image length and data processing constraints.

Nonetheless, this remains a useful analysis method for laboratory work, OAPs deployed on light aircraft with lower than ordinary airspeeds, and, because of the increased common size range, comparisons with forward scattering spectrometer probes.

Acknowledgments. This work was supported by the Natural Environment Research Council, under Studentship Award GT 04/99/AS/284.

REFERENCES

Brown, P. R. A., and P. N. Francis, 1995: Improved measurements of the ice water content in cirrus using a total-water probe. *J. Atmos. Oceanic Technol.,* **12,** 410–414.

Curry, M. J., and R. S. Schemenauer, 1979: The small particle response of an optical array precipitation probe. *J. Appl. Meteor.,* **18,** 816–821.

Gayet, J. F., P. R. A. Brown, and F. Albers, 1993: A comparison of in-cloud measurements obtained with 6 PMS 2DC probes. *J. Atmos. Oceanic Technol.,* **10,** 180–194.

Heymsfield, A. J., and D. Baumgardner, 1985: Summary of a workshop on processing 2-D probe data. *Bull. Amer. Meteor. Soc.,* **66,** 437–440.

Hovenac, E. A., and E. D. Hirleman, 1991: Use of rotating pinholes and reticules for calibration of cloud droplet instrumentation. *J. Atmos. Oceanic Technol.,* **8,** 166–171.

Jensen, J. B., and H. Granek, 2002: Optoelectronic simulation of the PMS 260X optical array probe and application to drizzle in a marine stratocumulus. *J. Atmos. Oceanic Technol.,* **19,** 568–585.

Knollenberg, R. G., 1970: The optical array: An alternative to scattering or extinction for airborne particle size determination. *J. Appl. Meteor.,* **9,** 86–103.

Korolev, A. V., S. V. Kuznetsov, Y. E. Makarov, and V. S. Novikov, 1991: Evaluation of measurements of particle-size and sample area from optical array probes. *J. Atmos. Oceanic Technol.,* **8,** 514–522.

——, J. W. Strapp, and G. A. Isaac, 1998: Evaluation of the accuracy of PMS optical array probes. *J. Atmos. Oceanic Technol.,* **15,** 708–720.

Lawson, R. P., and R. H. Cormack, 1995: Theoretical design and preliminary tests of two new particle spectrometers for cloud microphysics research. *Atmos. Res.,* **35,** 315–348.

——, A. V. Korolev, S. G. Cober, T. Huang, J. W. Strapp, and G. A. Isaac, 1998: Improved measurements of the drop size distribution of a freezing drizzle event. *Atmos. Res.,* **47–48,** 181–191.

Reuter, A., and S. Bakan, 1998: Improvements of cloud particle sizing with a 2D-Grey probe. *J. Atmos. Oceanic Technol.,* **15,** 1196–1203.

Strapp, J. W., F. Albers, A. Reuter, A. V. Korolev, U. Maixner, E. Rashke, and Z. Vukovic, 2001: Laboratory measurements of the response of a PMS OAP-2DC. *J. Atmos. Oceanic Technol.,* **18,** 1150–1170.